

# Effect of Various Overlap Distance in Waist Enlarged Tapers in Mach Zehnder Interferometer Fiber Optic Sensor for Liquid Temperature Monitoring

**Abstract.** A fiber optic sensor (FOS) based on the Mach-Zehnder interferometer (MZI) suitable for monitoring the liquid temperature is proposed and demonstrated. The sensor head was formed by a single mode-multimode-single mode (SMS) fiber structure through arc fusion splicing. The intermodal interference is achieved by two waist-enlarged tapers (WET) at the coupling points of the multimode fiber (MMF) and single mode fibers (SMF). The sensitivity of the sensor was determined based on the overlap distance for waist enlargement, tested in different temperatures of liquid. Five different overlap distances set in the conventional fiber splicer were 30  $\mu\text{m}$ , 60  $\mu\text{m}$ , 90  $\mu\text{m}$ , 120  $\mu\text{m}$  and 150  $\mu\text{m}$ . The highest sensitivity of 0.0984  $\text{nm}/^\circ\text{C}$  was produced by the SMS sensor with overlap distance of 150  $\mu\text{m}$ . Such easily fabricated, cost-effective and temperature-immune fiber interferometer could be used for high temperature sensing applications. Manipulation of the overlap distance contributes to the advancement of the device.

**Streszczenie.** Zaproponowano i zademonstrowano czujnik światłowodowy (FOS) oparty na interferometrze Mach-Zehnder (MZI) odpowiedni do monitorowania temperatury cieczy. Głowica czujnika została utworzona przez strukturę włókna jednomodowego-wielomodowego-jednomodowego (SMS) poprzez spawanie lukowe. Intermodalność intermodalna jest uzyskiwana dzięki dwóm zwężeniom powiększonym w talii (WET) w punktach łączenia włókien wielomodowych (MMF) i jednomodowych (SMF). Czulość czujnika została określona na podstawie odległości zakładki dla powiększenia talii, badanej w różnych temperaturach cieczy. Pięć różnych odległości nakładania ustawionych w konwencjonalnej spawarce włókien wynosiło 30  $\mu\text{m}$ , 60  $\mu\text{m}$ , 90  $\mu\text{m}$ , 120  $\mu\text{m}$  i 150  $\mu\text{m}$ . Największą czulość 0,0984  $\text{nm}/^\circ\text{C}$  uzyskał czujnik SMS z odległością nakładania 150  $\mu\text{m}$ . Taki łatwy w produkcji, opłacalny i odporny na temperaturę interferometr światłowodowy może być używany w aplikacjach z czujnikami wysokiej temperatury. Manipulacja odległością nakładania się przyczynia się do postępu urządzenia. (Wpływ różnych odległości zachodzenia na siebie w powiększonych zwężeniach talii w czujniku światłowodowym Mach Zehnder Interferometer do monitorowania temperatury cieczy)

**Keywords:** Fiber optic sensor, Mach Zehnder Interferometer, waist enlarged tapers, overlap distance, liquid temperature monitoring

**Słowa kluczowe:** czujniki światłowodowe, interferometr

## Introduction

It is essential to monitor the environment parameter such as temperature, pressure and humidity in many areas of commerce and everyday life such as oil & gas industry, weather observation and agriculture fields. The detection devices are required to be small size, electromagnetic immunity and resistance to corrosive and hazardous environment.

Fiber optic sensors (FOS) has been utilized in various application due to its versatility [1]–[3]. The FOS as temperature sensor has been extensively studied over the years. The FOS could satisfy the requirement to be the superior detection devices compared to the conventional electrical temperature sensors. Different types of fiber optic as temperature sensor has been proposed such as fiber Bragg grating (FBG)[4], long period grating (LPG) [5], fiber interferometers [5], [6], U-bend fiber structure [7], tapered fiber[8] and photonic crystal fiber (PCF) structure [9].

Previous research has reported different types of interferometer, which includes the Michelson interferometer (MI), Fabry-Perot interferometer (FPI), Mach-Zehnder interferometer (MZI) and Sagnac interferometer (SI). Nevertheless, the fabrication of MI resulted in partial reflection of the lead-in optical signals as in [10]. Meanwhile, FPI reported low sensitivity performance [11]. The researcher in [11] discussed drawback of SI in terms of the sensitivity of the polarization mirror. Generally, the limitations lead to the increase of cost. Therefore, MZI offers advantages such as in terms of cost and flexibility of configurations [12].

Hence this paper proposed MZI as the FOS by using singlemode-multimode-singlemode (SMS) based on Waist-Enlarged Tapers (WET) structure. The fabrication technique for this structure is based on the simple fusion splicing

technique compared to other fabrication methods of MZI structure such as by using a dispersion compensation fiber [13], no core fiber [14] and nano-coating technology [15]. These methods require accurate processes and special equipment to fabricate the sensor. The WET structure were formed by overlapping the splicing distance of the SMF and MMF thus forming an elliptical core area in the centre of WET.

The FOS for sensing temperature based on SMS with WET structure with different overlap distances for waist-enlarged tapers were proposed and experimentally demonstrated. Every sensor consists of two waist-enlarged tapers fabricated using commercial splicer. The difference between the sensors are the waist enlargement size determined by the overlap distance ranging from 30  $\mu\text{m}$  to 150  $\mu\text{m}$  to study its effect towards the sensors performance. It is observed that manipulation of the overlap distance resulted to a better performance of the device.

## Principal of The Device

Figure 1 depicts the schematic diagram of the proposed MZI structure which consists of two WET structures in between the spliced single mode fiber (SMF) and the multimode fiber (MMF). Theoretically, the light travels from SMF is split into two directions which is into core and cladding region when it passes through WET. So, the light propagate in cladding modes will react with substance which surrounding the cladding. The split light is then recoupled back and interfere with mode by the second WET, which consequently forms the intermodal MZ interferometer. An elliptical core area is formed in the center of WET which leads to light coupling into the cladding easily. The waist diameter, waist length of the WET is represented by  $d$  and  $l$  respectively. Meanwhile,  $L$  refers to the sensing area of the device.

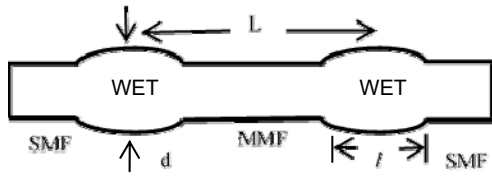


Fig.1. Schematic diagram of the SMS based on WET structure

The difference between the value of the cladding's refractive index and the external medium's refractive index determines the effective index of the cladding modes. Although the core of the SMF is exposed to the external environment, some of the optical signal still being transmitted [16]. By considering the core and cladding mode, the transmission spectrum of the interferometer is expressed as:

$$(1) \quad I = I_1 + I_2 2\sqrt{I_1 I_2} \cos \left[ \frac{2\pi(n_{co}^{eff} - n_{cl}^{eff}) L}{\lambda} \right]$$

where  $I_1$  and  $I_2$  are the light intensities of the core mode and the cladding mode,  $\lambda$  is the free-space optical wavelength in air,  $L$  is the length of the thin-core fiber, and  $n_{co}^{eff}$ ,  $n_{cl}^{eff}$  are indexes of the core and cladding. The wavelength of the interference is expressed as:

$$(2) \quad \lambda = \left[ \frac{2\pi(n_{co}^{eff} - n_{cl}^{eff}) L}{2k + 1} \right]$$

Based on the equations, the parameters which changes the fiber length and the effective refractive index of fiber cladding and core fiber can be determined. Since there is an effect on the refractive index differences between the MMF cladding and core modes, an interference pattern could be expected by measuring the transmission spectrum of the device.

A large free spectral range (FSR) should be obtained as a result of the potential interference forms made by the contacts among the SMF's higher order modes. The phase change concerning the core and the cladding modes after transmission through MMF of length  $L$  can be expressed as:

$$(4) \quad \phi^m = \frac{2\pi(n_{eff}^{core} - n_{eff}^{cladding,m})}{\lambda} L = \left[ \frac{2\pi(n_{co}^{eff} - n_{cl}^{eff})}{\lambda} L \right]$$

where  $\Delta n_{eff}^m$  is the effective refractive index between the core mode and  $m$ th cladding mode.  $\lambda$  represents the input wavelength. Based on Eq. (4), the wavelength separation between two interference minima (the FSR) can be approximated as:

$$(5) \quad \Delta\lambda \approx \left[ \frac{\lambda^2}{\Delta n_{eff}^m L} \right]$$

The relation of the FSR and the interferometer is inversely proportional [17].

### Waist Enlarged Tapers (WET)

Firstly, the polymer coating of multimode fiber, MMF and single mode fiber, SMF was stripped off about 25 mm using fiber optic cable stripper. Then, the fiber was cleaned with alcohol to make sure it is free from dust. Later, every end of the fiber, SMF and MMF was cleaved off using high-quality cleaver Fujikura CT-30 to obtain flat end faces.

The Fujikura FSM-18R was utilized to form the WET structure between SMF and MMF. The overlap distance was set so that SMF and MMF were pushed further towards each other during the splicing process. After the arc discharge, the fiber diameter was gradually enlarged due to the pushing force and the overlap. Finally, another section of the Waist-Enlarged was created at another end of the MMF connected with SMF using the same splicer procedure.

The analysis was conducted towards five different overlap distances which created different length and diameter of the WET. The overlap distance for the sensor analysed were 30  $\mu\text{m}$ , 60  $\mu\text{m}$ , 90  $\mu\text{m}$ , 120  $\mu\text{m}$  and 150  $\mu\text{m}$ . Figure 2 and 3 displays the image of the splicing process obtained from the Image Analyzer for normal splicing and WET structure with overlap distance of 150  $\mu\text{m}$ .

Meanwhile, the relationship between the overlap distance and the diameter and length of WET are depicted in Figure 4 and 5 respectively. It is observed that as the overlap distance increases from 30  $\mu\text{m}$  to 150  $\mu\text{m}$ , the diameter,  $d$  of the WET increases. Similar pattern was observed for the length of the WET. Thus, it is concluded that the size of ellipse shape of WET grows bigger as the overlap distance increases. The overlap distance applied creates pushing force resulting in the ellipse shape of WET. The maximum overlap distance set in commercial splicer which was 150  $\mu\text{m}$  produced maximum WET diameter and length with 140  $\mu\text{m}$  and 428  $\mu\text{m}$  respectively.

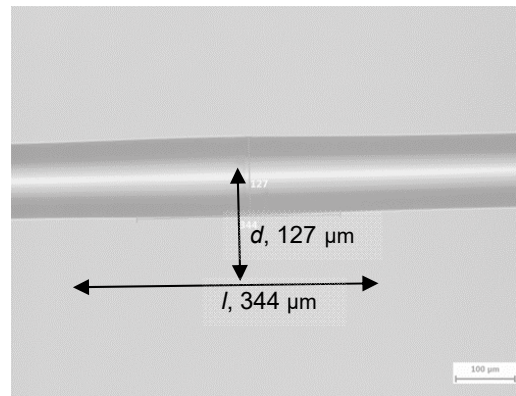


Fig.2. Measurement of ellipse shape of normal splicing

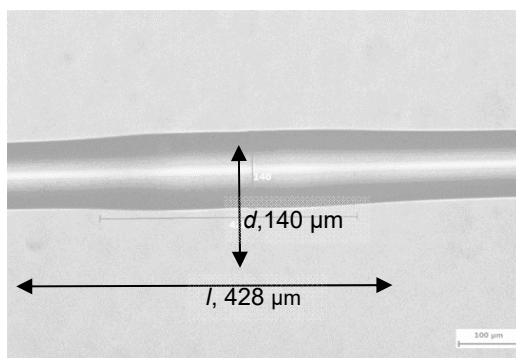


Fig.3. Measurement of ellipse shape of WET with overlap distance of 140  $\mu\text{m}$

### SMS Based on WET As A Liquid Temperature Sensor

The SMS structure of WET with different overlap distance (30  $\mu\text{m}$ , 60  $\mu\text{m}$ , 90  $\mu\text{m}$ , 120  $\mu\text{m}$  and 150  $\mu\text{m}$ ) were then characterized as a liquid temperature sensor.

The experimental setup is displayed in Figure 6. The first SMF was connected to the optical light source (1310 nm, 10 mW). Meanwhile the second SMF was connected to the optical spectrum analyser (OSA). The sensor was

tested in oil with room temperature which is 30°C and the value of the resonant wavelength was made as the reference value. After the reference value was obtained, the sensors were tested in oil with different temperature. The oil was heated using heater to vary the temperature from 30°C to 100°C. The procedure was repeated with other SMS sensors which has different overlap distance. The experiment was repeated three times in order to get the average output reading.

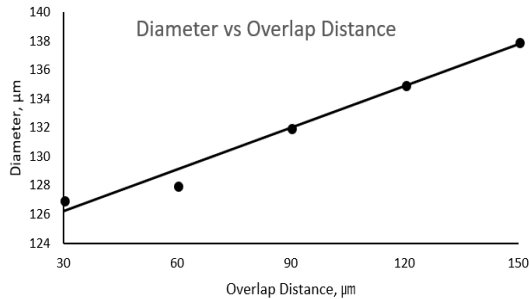


Fig. 4. Linear fitting regression graph of diameter vs overlap distance

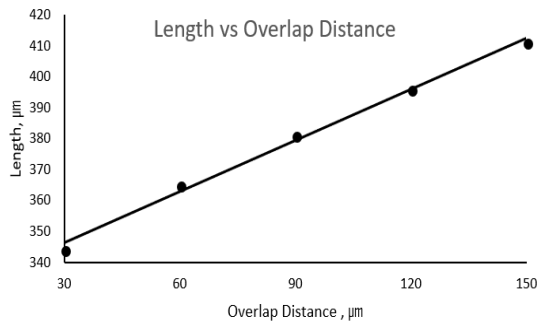


Fig. 5. Linear fitting regression graph of length vs overlap distance

Then, the resonant wavelength shift was calculated by subtracting the output wavelength shift and the reference output wavelength. The resonant wavelength shift versus temperature graphs were plotted to acquire the sensitivity. The value of the sensitivity of the sensor was obtained from the slope of the graph.

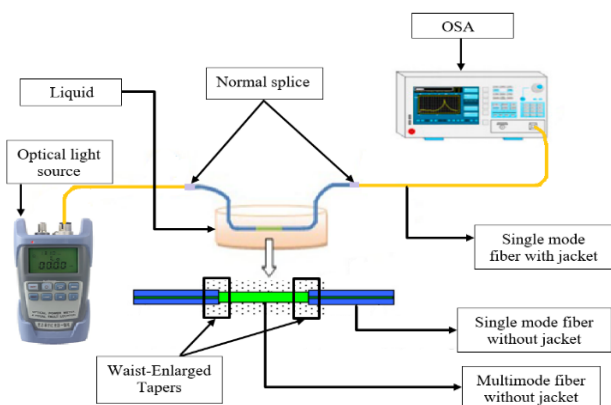


Fig. 6: Experimental setup of the project

### Performance of SMS based on WET as a liquid temperature sensor

Figure 7 shows the average output wavelength over temperature for five SMS sensors with different overlap distances which are 30 µm, 60 µm, 90 µm, 120 µm and 150 µm. The resonant wavelength shift was calculated by determining the difference between output wavelength shift and reference output wavelength. From Figure 7, SMS

sensor with overlap distance 150 µm has the highest slope which means every increment of 10°C the output wavelength is ascending the most. The lowest slope was produced from SMS sensor with overlap distance 30 µm. This is due to the slight increase of the wavelength for every 10°C. The resonant wavelength for SMS sensor for 30 µm overlap distance is 1314.15 nm at 30°C and 1316.68 nm at maximum temperature which is 100°C.

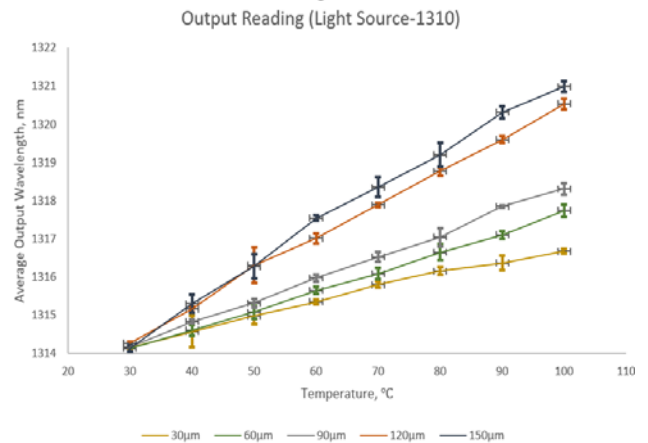


Fig. 7: Linear fitting regression graph of diameter vs overlap distance

The resonant wavelength shift is displayed in Figure 8. The wavelength shifts for the sensor with 30 µm overlap distance was the smallest with only 2.73 nm while the maximum highest wavelength shift was produced by SMS sensor with 150 µm overlap distance recorded a wavelength shift of 6.86 nm. It is observed that the SMS sensor with overlap distance of 150 µm has the highest slope. The lowest slope was produced from SMS sensor with overlap distance of 30 µm. This is due to the slight increase of the wavelength for every 10°C.

Meanwhile, the SMS sensor with 150 µm overlap distance has the highest slope which represents the sensitivity value of 0.0984 nm/°C. The lowest sensitivity was produced by SMS sensor with 30 µm overlap distance which is 0.0397 nm/°C or 39.7 µm/°C. It can be concluded that the overlap distance affects the sensitivity of the SMS sensor. The larger the overlap distance, the higher the sensitivity of SMS sensor. The phenomenon might be due to the fact that when the overlap distance is longer, bigger elliptical core area in the center of WET is formed, therefore it is possible to excite and recouple more cladding modes with the fundamental mode [6].

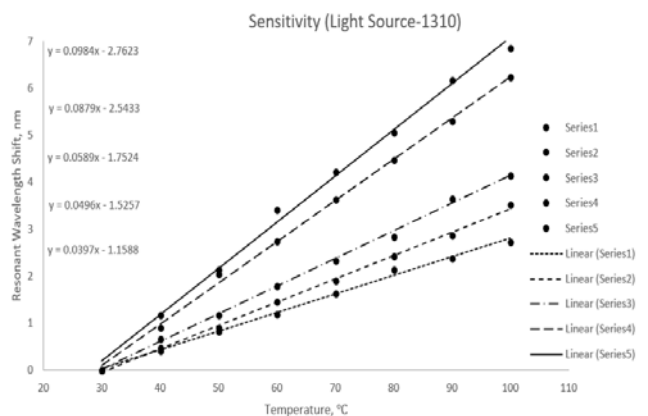


Fig. 8: Resonant wavelength shift vs temperature

## Conclusion

In conclusion, this simple, cost effective waist-enlarged tapers affect the performance of the SMS fiber optic sensor in terms of the sensitivity of the device. The fiber optic sensor has been fabricated by single mode-multimode-single mode (SMS) structure with two WET as connection between single mode and multimode. The SMS fiber optic sensor was tested in oil with varied temperature from 30°C to 100°C. The sensitivity produced by SMS fiber optic sensor is in the range of 0.026nm/°C to 0.0984nm/°C. The highest sensitivity of SMS fiber optic sensor reported in this work, which is which is 0.0984 nm/°C performs better than previous work in [18] with 0.0709 nm/°C. This work demonstrates that the better performance of the device is made possible by manipulating the overlap distance of the WET.

## Acknowledgment

The authors would like to thank Universiti Teknikal Malaysia Melaka (UTeM) for the support on the research.

**Corresponding Author:** Dr. Hanim Abdul Razak, Centre for Telecommunication Research & Innovation (CeTRI), Faculty of Electronics Engineering and Computer Engineering, Universiti Teknikal Malaysia Melaka, Hang Tuah Jaya, 76100 Durian Tunggal, Melaka. E-mail: hanim@utem.edu.my

## REFERENCES

- [1] H. A. Razak, N. H. Sulaiman, H. Haroon, and A. S. Mohd Zain, "A fiber optic sensor based on Mach-Zehnder interferometer structure for food composition detection," *Microw. Opt. Technol. Lett.*, vol. 60, no. 4, 2018
- [2] Y. Noh *et al.*, "Image-Based Optical Miniaturized Three-Axis Force Sensor for Cardiac Catheterization," *IEEE Sens. J.*, vol. 16, no. 22, pp. 7924–7932, Nov. 2016
- [3] G. B. Kashaganova, P. Komada, and G. Karnakova, "Fiber sensors based on the Bragg gratings in security systems," *Prz. Elektrotechniczny*, vol. 96, no. 9, 2020
- [4] F. Ahmed, V. Ahsani, A. Saad, and M. B. G. Jun, "Bragg grating embedded in Mach-Zehnder interferometer for refractive index and temperature sensing," *IEEE Photonics Technol. Lett.*, vol. 28, no. 18, pp. 1968–1971, 2016
- [5] L. Cai, Y. Zhao, and X. G. Li, "Applications of modal interferences in optical fiber sensors based on mismatch methods," *Instrumentation Science and Technology*, vol. 43, no. 1, pp. 1–20, 2015
- [6] M. Shao, X. Qiao, H. Fu, H. Li, J. Zhao, and Y. Li, "A Mach-Zehnder interferometric humidity sensor based on waist-enlarged tapers," *Opt. Lasers Eng.*, vol. 52, no. 1, pp. 86–90, 2014
- [7] B. H. Lee *et al.*, "Interferometric fiber optic sensors," *Sensors*, vol. 12, no. 3, pp. 2467–2486, 2012
- [8] J. Shi, S. Xiao, L. Yi, and M. Bi, "A sensitivity-enhanced refractive index sensor using a single-mode thin-core fiber incorporating an abrupt taper," *Sensors*, vol. 12, no. 4, pp. 4697–4705, 2012
- [9] J. Villatoro, V. Finazzi, G. Badenes, and V. Pruneri, "Highly sensitive sensors based on photonic crystal fiber modal interferometers," *J. Sensors*, vol. 2009, 2009
- [10] J. Zhou *et al.*, "Intensity modulated refractive index sensor based on optical fiber Michelson interferometer," *Sensors Actuators, B Chem.*, 2015
- [11] X. hu Fu *et al.*, "A tension insensitive PbS fiber temperature sensor based on Sagnac interferometer," *Optoelectron. Lett.*, 2017
- [12] A. R. Hanim *et al.*, "Modeling Mach Zehnder Interferometer (MZI) modulator on silicon-on-insulator (SOI)," *J. Telecommun. Electron. Comput. Eng.*, vol. 8, no. 1, 2016.
- [13] F. Wang, L. Zhang, T. Ma, X. Wang, K. Yu, and Y. Liu, "A high-sensitivity sensor based on tapered dispersion compensation fiber for curvature and temperature measurement," *Opt. Commun.*, vol. 481, 2021
- [14] C. Li *et al.*, "Liquid level measurement based on a no-core fiber with temperature compensation using a fiber Bragg grating," *Sensors Actuators, A Phys.*, vol. 245, 2016
- [15] P. J. Rivero, J. Goicoechea, and F. J. Arregui, "Layer-by-layer nano-assembly: A powerful tool for optical fiber sensing applications," *Sensors (Switzerland)*, vol. 19, no. 3, 2019
- [16] J. Villatoro and D. Monzón-Hernández, "Low-cost optical fiber refractive-index sensor based on core diameter mismatch," *J. Light. Technol.*, vol. 24, no. 3, pp. 1409–1413, 2006
- [17] H. Sun *et al.*, "Temperature and refractive index sensing characteristics of an MZI-based multimode fiber-dispersion compensation fiber-multimode fiber structure," *Opt. Fiber Technol.*, vol. 18, no. 6, pp. 425–429, 2012
- [18] H. Wang *et al.*, "Simultaneous measurement of refractive index and temperature based on asymmetric structures modal interference," *Opt. Commun.*, vol. 364, pp. 191–194, 2016